

PAPER • OPEN ACCESS

## On the behavior of auxetic inserts: a numerical analysis to derive design guidelines

To cite this article: Diego Di Brizzi *et al* 2024 *Smart Mater. Struct.* **33** 075018

View the [article online](#) for updates and enhancements.

### You may also like

- [Auxetic mechanical metamaterials: from soft to stiff](#)  
Xiang Li, Weitao Peng, Wenwang Wu et al.
- [Deep reactive ion etching of auxetic structures: present capabilities and challenges](#)  
Alban Muslija and Andrés Díaz Lantada
- [Lithography-based ceramic manufacture \(LCM\) of auxetic structures: present capabilities and challenges](#)  
Andrés Díaz Lantada, Adrián de Blas Romero, Martin Schwentenwein et al.



**HONOLULU, HI**  
October 6-11, 2024

*Joint International Meeting of*  
The Electrochemical Society of Japan (ECSJ)  
The Korean Electrochemical Society (KECS)  
The Electrochemical Society (ECS)







Early Registration Deadline:  
**September 3, 2024**

**MAKE YOUR PLANS NOW!**



# On the behavior of auxetic inserts: a numerical analysis to derive design guidelines

Diego Di Brizzi<sup>1</sup> , Serena Graziosi<sup>1,\*</sup> , William Bondin<sup>2</sup>, Joseph N Grima<sup>3</sup>   
and Alessandro Airoidi<sup>4</sup> 

<sup>1</sup> Department of Mechanical Engineering, Politecnico di Milano, Via La Masa 1, 20156 Milan, Italy

<sup>2</sup> I+A, Triq San Guzepp 17, Tarxien, TXN 1024, Malta

<sup>3</sup> Department of Chemistry/Metamaterials Unit, Faculty of Science, University of Malta, Msida, MSD 2080, Malta

<sup>4</sup> Department of Aerospace Science and Technology, Politecnico di Milano, Via La Masa 34, 20156 Milan, Italy

E-mail: [serena.graziosi@polimi.it](mailto:serena.graziosi@polimi.it)

Received 23 February 2024, revised 16 May 2024

Accepted for publication 21 May 2024

Published 13 June 2024



## Abstract

Auxetics are a class of materials and metamaterials with a negative Poisson's ratio ( $\nu$ ) and have gained tremendous popularity over the last three decades. Many studies have focused on characterizing designs that allow obtaining a negative  $\nu$ . However, some open issues remain concerning understanding the auxetic behavior in operational conditions. Studies have been centered on analyzing the response of specific auxetic topologies instead of treating auxeticity as a property to be analyzed in a well-defined structural context. This study aims to contribute to the investigation of auxetic materials with a structural application, focusing on maximizing performance. The field of application of auxetics for designing inserts was selected and a model of a nail-cavity system was created to determine the effects of different design choices on the system behavior by exploring relationships between selected parameters and the auxetic insert behavior. The exploration combines finite element modeling analyses with their surrogate models generated by supervised learning algorithms. This approach allows for exploring the system's behavior in detail, thus demonstrating the potential effectiveness of auxetics when used for such applications. A list of design guidelines is elaborated to support the exploitation of auxetics in nail-cavity systems.

Supplementary material for this article is available [online](#)

Keywords: auxetic structures, finite element method, regression models, insert, nail

\* Author to whom any correspondence should be addressed.



Original content from this work may be used under the terms of the [Creative Commons Attribution 4.0 licence](#). Any further distribution of this work must maintain attribution to the author(s) and the title of the work, journal citation and DOI.

## 1. Introduction

In recent years, mainly thanks to the developments in manufacturing techniques such as Additive Manufacturing (AM), there has been a growing interest in mechanical metamaterials, structures, or ‘architected materials’ exhibiting peculiar responses to external stimuli [1]. These unusual behaviors result from the synergic contribution of the raw material arrangement in the design space (geometry) and how the design responds to stimuli (the deformation mechanism). One of the main areas being studied is related to the auxetics [2], which are systems that exhibit a negative Poisson’s ratio ( $\nu$ ) [3, 4]. A negative  $\nu$  causes the material to expand along the transverse direction when uniaxially pulled and to shrink when compressed [5]. Therefore, a negative  $\nu$  imparts a completely different response to deformation than conventional materials, typically characterized by a positive  $\nu$  value. The interest in auxetics derives from the will to explore unconventional deformation mechanisms and to discover and utilize the positive collateral effects of a negative  $\nu$  [3]. For example, it is already proven that the negative  $\nu$  of auxetic materials leads to superior shear, indentation, impact, tensile fatigue, and fracture resistance [5–13]. It increases energy absorption abilities and provides synclastic curvature properties [9, 14–21]. Such enhanced properties make auxetics ideal for various applications, such as in the biomedical field, seismic materials, textile and sports equipment production, and automotive and aerospace industries [9, 18, 22–30].

Depending on the number of planes along which the negative  $\nu$  is exhibited, a material will be referred to as fully auxetic or partially auxetic or as a 2D, a 3D, or a quasi-two-dimensional (Q2D) auxetic [31–34]. Nowadays, research has already widely explored geometric solutions to drive their design, even if there is no established fabrication method for auxetics at a large scale characterized by complex 3D topologies [35]. As previously mentioned, the growth in the field of auxetics is also linked to the development of AM processes. They allow the printing of porous structures conceived from both stochastic material arrangement and the periodic repetition of a unit cell, which acts as the main building block [36]. The cell geometry defines the deformation mechanism of the whole structure, thanks to its scale-independent nature [37, 38]. However, this concept of cell repetition is just one of many possible manufacturing solutions, as there are also several studies on the production, modeling, and characterization of foams able to exhibit a negative  $\nu$  [18, 23, 39]. Regardless of the manufacturing process, auxetics’ mechanical properties depend on the structure’s geometry and how it deforms when subjected to loads [40]. For this reason, over the years, most of the research effort has been put into designing and characterizing different classes of structures, generating a large pool of potential auxetic designs [35, 36, 41–47].

The current scientific literature on auxetics considered as bulk is still developing, particularly with auxetics employed in a structural role, partly due to the minimal presence of bulk auxetics in natural or artificial form. However, despite these advancements, the possibilities offered by the

peculiar deformation mechanisms of auxetic materials and meta-materials have still to be explored for many engineering applications. To further boost the spread of this type of auxetics, deepening the advantages and drawbacks of a negative Poisson’s ratio response from a high-level perspective that does not focus on specific topologies or technological solutions is necessary. Indeed, instead of focusing on the behavior of any design, evaluations on auxetics themselves are needed to provide a broader perspective on the subject. Despite the lack of existing bulk auxetics, these evaluations could be performed by considering a purely numerical model of a negative Poisson material having homogenized properties. This is not a limitation for a study focused on providing a high-level understanding of the behavior of auxetics, as it would contribute to setting the requirements for future developments of specific auxetic materials and metamaterials. This numerical and homogenized approach allowed us to investigate the optimal combinations of material parameters that could improve the structural performance of an auxetic material in different engineering applications. Hence, the present work aims to provide a bridge between the engineering requirements of the application scenario and the properties of the auxetic metamaterials that can optimize the performance of the system at the engineering level. Such a point of view is rarely adopted in current scientific literature. However, it is deemed fundamental to stimulate and drive the advancement of research in the auxetic material field.

A potential application field for auxetics, already explored in literature, is their use as reversible mechanical joints or fasteners. Their ability to shrink in two directions simultaneously and their tendency to expand under tension could make them easy to push into a cavity and hard to pull out from, which is the condition for a well-performing joint. Introducing a fastener that can work without applying glue may constitute a relevant solution in multiple fields. For instance, furniture production would benefit from a completely reversible fixation system. Moreover, the biomedical field has sought joint systems, like screws, for orthopedic treatments. Even if they would allow an increase in fixation strength, the risk of causing damage to the surrounding tissue could be too high to take. Auxetic materials could be an effective solution. By expanding under tension, they should enhance the fixation strength. At the same time, their ability to resume deformation would prevent them from causing damage to the surrounding tissue [48].

However, experimental results from previous studies demonstrated that auxetic fasteners’ performances are not necessarily good enough to be considered a valuable option [30, 49]. Some studies have confirmed the ease of insertion for auxetic nails, but the overall behavior through the insertion-extraction cycle has not yet been deeply analyzed [50]. Besides, previous studies on auxetic fasteners are mainly based on cylindrical models inspired by a conventional insert’s shape [30, 48, 49]. There is no clear evidence that the cylindrical configuration is the best-performing one for an auxetic nail-like insert (henceforth, without loss of generality, referred to simply as ‘nail’).

The contribution of our study is thus twofold. First, it explains how specific geometric- and material-related nail-cavity system parameters influence the mechanical behavior of auxetic fasteners. The auxetic insert is treated as bulk, and manufacturing-related aspects were intentionally not considered. Second, a methodology is proposed to explore such behavior further and develop it. A 6400-simulation database has been created and used as input to train a supervised learning algorithm. Regression models describing the effects of the variable combinations on the system behavior were generated and leveraged to elaborate design guidelines. These regressions were used as surrogate models for the Finite Element (FE) simulations [51]. This approach is widely used to conduct analyses on multi-parameter models at a reduced computational cost without requiring time- and resource-consuming simulations [52–54].

## 2. Materials and methods

The FE models of a bulk auxetic, treated as a fastener in an insertion-extraction cycle from a cavity dug in a conventional ( $\nu > 0$ ) material, were developed using Simulia/Abaqus Standard 2020 (Dassault Systèmes) non-linear implicit simulations. All the implementing details are provided in the Supporting Information, while an overview of its main elements and parameters is provided in figure 1.

The nail and the cavity were modeled as solids of revolution (figure 1(a)), allowing for employing a 2D axisymmetric model (figure 1(c)) to optimize computing time. Figure 1(b) shows the material (assumed to be isotropic) and geometric parameters considered in this study. The following sections discuss these parameters and why they were selected to explore the behavior of a nail-cavity system.

### 2.1. Parameters included in the analysis

The geometric and material-related parameters (figure 1(b)) considered in this study are overviewed hereby and summarized in table 1.

The Poisson's ratio of the cavity ( $\nu_{\text{cav}}$ ) has been intentionally set to 0.4, a value typical for several materials. For the Poisson's ratio of the auxetic (i.e.  $\nu_{\text{nail}}$ ), values ranged from  $-0.9$  to  $-0.1$ , covering the whole auxetic range for isotropic materials (details on how the homogenized auxetic behavior was implemented in the FE model are provided in section S1.1 of the supporting information). They were considered with a 0.01 discretization (table 1). A comparison between auxetic nails and conventional ones has also been made. For the conventional nail,  $\nu_{\text{c-nail}}$  was set to 0.3. The  $\alpha$  parameter has been used to define both bodies' geometry and limit the number of variables considered. It ranges from  $91^\circ$  to  $102^\circ$ , with  $0.1^\circ$  discretization (table 1). Lower values would not have allowed using a nail with a larger radius than the cavity (further explanations are provided later). Values larger than  $102^\circ$  would have caused excessive nail distortion when entering the cavity. The radius of the cavity ( $R_{\text{cav}}$ ) has been kept constant at an arbitrary value of 13 mm (table 1) to reduce the number of variables in

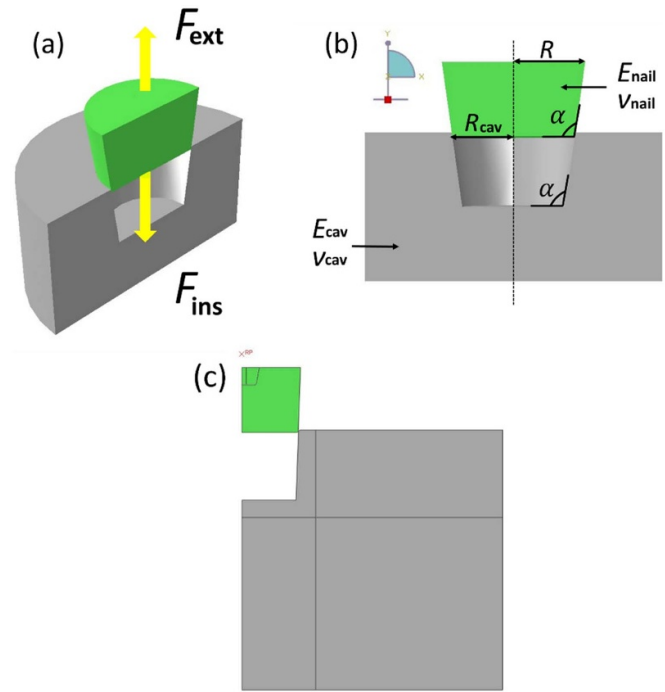


**Figure 1.** Nail-cavity (green and grey, respectively) system solid models and parameters. (a): Simulia/Abaqus Standard 2020 assembly representing an auxetic nail and a cavity as solids of revolution where ' $F_{\text{ins}}$ ' is the insertion force and ' $F_{\text{ext}}$ ' is the extraction one. (b): Parameters included in the analysis:  $\nu_{\text{nail}}$  is the nail's Poisson's modulus,  $\nu_{\text{cav}}$  the cavity's Poisson's modulus,  $\alpha$  is the tapering angle,  $R_{\text{nail}}$  the nail's radius,  $R_{\text{cav}}$  the cavity's radius,  $E_{\text{nail}}$  the nail's Young modulus and  $E_{\text{cav}}$  the cavity's Young modulus. (c): The axisymmetric model employed to perform the FE analyses.

**Table 1.** Range values assigned to the different parameters shown in figure 1(b).

	Lower bound	Upper bound	Discretization
$\nu_{\text{nail}}$	$-0.9$	$-0.1$	0.01
$\alpha$	$91^\circ$	$102^\circ$	0.1
$R_{\text{nail}}$ (mm)	13.5	15	0.1
Discrete values			
$E_{\text{nail}}$ (MPa)	19, 250, 750, 1500		
$E_{\text{cav}}$ (MPa)	250, 750, 1500, 206 000		
$\nu_{\text{c-nail}}$	0.3		
$\nu_{\text{cav}}$	0.4		
$R_{\text{cav}}$ (mm)	13		

the analysis and to consider  $R_{\text{nail}}$  as an indicator of the 'mechanical interference' between the nail and the cavity. Therefore, for a more straightforward comprehension of the parameter's effect,  $R_{\text{nail}}$  has been mathematically treated as a ratio to  $R_{\text{cav}}$ :

$$\delta = \left( \frac{R_{\text{nail}}}{R_{\text{cav}}} - 1 \right) \times 100. \quad (1)$$

This ratio (equation (1)) quantifies the nail-cavity interference based on the selected dimensions. The minimum value for  $R_{\text{nail}}$  was set to 13.5 mm (table 1). This value should be

seen as a starting condition. There are no specific and relevant reasons for this selection. In comparison, the maximum was arbitrarily fixed at 15 mm with a discretization of 0.1 mm (table 1). Therefore,  $\delta$  ranged from 3.8% to 25%. The lower boundary was set to higher values than  $R_{cav}$  to induce the nail's compression. The upper boundary was limited to 15 mm to prevent the nail from excessively distorting when entering the cavity. The Young moduli of the nail ( $E_{nail}$ ) and the cavity ( $E_{cav}$ ) were treated independently one from the other and through their ratio:

$$\gamma = \frac{E_{nail}}{E_{cav}}. \quad (2)$$

This ratio (equation (2)) is indeed a further aspect that a design engineer could consider when dimensioning a nail-cavity system. Possible values for both variables were arbitrarily chosen among the elastic moduli of existing materials (spanning through different polymers for the nail, going from polymers to steel-like materials for the cavity), as synthesized in table 1 (more details on the material model set in Simulia/Abaqus Standard 2020 are provided in sections S1.1–S1.3 of the supporting information). This choice allowed us to formulate the research results, considering possible applications. However, it is essential to highlight that if the auxetic nail is no longer a solid bulk but a cellular structure, its Young modulus is expected to be lower than its base material [49]. Therefore, in that case, its shape, relative density, and material should be chosen to obtain the desired  $E_{nail}$  value.

Besides, it is worth clarifying that, for each parameter, the ranges of their possible values were selected according to geometric, material, and computational constraints. Among the geometric limitations is the one deriving from the relationship between  $\alpha$  and  $R_{nail}$ . Indeed,  $R_{cav}$  (figure 1(b)) must be larger than the radius of the bottom of the nail. Otherwise, the nail cannot enter the cavity without undergoing extensive distortion. Therefore, for a certain  $R_{nail}$ , there is a limitation to the minimum  $\alpha$  that can be considered. Vice versa, given certain  $\alpha$  values, that physical constraint limits the  $R_{nail}$  values.

Finally, it is worth clarifying that the friction coefficient was not added to the list of parameters as it would have heavily lifted the computational cost of the analysis. It has been kept constant at a value of 0.3. As a design variable, this coefficient raises or lowers the values of the forces involved in the insertion and extraction of the nail. The lack of this influence has not been considered to affect our parametric analysis's validity since the investigation focused on defining influence trends. Detailed quantitative evaluations were beyond the scope of the present work and left for future development.

## 2.2. The approach implemented to explore the parameters' influence

The impact of the parameters presented in section 2.1 was evaluated using non-linear implicit simulations. The approach adopts an implicit integration scheme to solve static non-linear problems. It faced some convergence issues for specific parameter values. For example, analyses with  $\nu_{cav} > 0.4$  and  $\delta > 25\%$  (equation (1)) could not be accomplished

with a reasonable number of increments due to the excessive distortion of the elements in the nail model. To address this issue, mesh refinements were tested without noteworthy improvements in making the solutions converge but with a significant increase in computational costs. An explicit model would have addressed this issue more effectively. However, this approach was avoided to maintain the required computational power and time to a level suitable for performing a parametric analysis with many simulations. As anticipated, a 6400-simulation database was generated. However, this issue has not limited the effectiveness of the study, and analyses on more extreme parameter ranges were considered a matter that could be addressed in future investigations.

During the analysis, the auxetic nail undergoes an insertion-extraction action into and from the cavity. This behavior is obtained by tying (through a Tie constraint available in the solver code) a rigid partition of the nail to a Reference Node (RP, see section S1.3 of the supporting information), whose motion along the nail axis (y-axis in figure 1(b)) is controlled by imposing it a displacement [55]. At the same time, the movement in the other two directions is fixed to zero. The numerical analyses were conducted to simulate an insertion-extraction process divided into three steps, characterized by different displacement boundary conditions assigned along the y direction of the RP linked to the nail. In the first step, the displacement was assigned to make the nail enter completely into the cavity. Thus, the nail's movement extension depends on the system's geometry. In the second step, the RP was released, and the nail started to move freely due to the force applied by the cavity. Such a step was deemed fundamental to understanding if the nail tended to be expelled from the cavity after the insertion phase. Finally, in the third step, a displacement was imposed on the RP in the outward direction to simulate extraction and measure the force required. The performance of each design configuration was evaluated by computing the changes in the reaction force values acting on RP. In particular, the evaluation was done by looking at the following ratio:

$$\eta = \frac{F_{ext}}{F_{ins}}. \quad (3)$$

This ratio  $\eta$  (equation (3)) between the maximum force required by the pull-out action ( $F_{ext}$ ) and the maximum force needed to push the nail in the cavity ( $F_{ins}$ ) is an efficiency parameter. The force values (i.e.,  $F_{ext}$  and  $F_{ins}$ ) are also important parameters because they strongly correlate to the specific field of application of the nail-cavity system to be designed.

After being checked with a mesh convergence analysis (see section S1.5), the model was used to perform a series of preliminary analyses and a parameter sensitivity study based on sets of simulations where each parameter was varied separately.

The preliminary analyses were run on models ( $M_1$  and  $M_2$ ) defined by intermediate values (table 2) compared to those available in table 1. The  $M_2$  model represents a conventional nail-cavity system because the nail has a positive Poisson's coefficient. The comparison between these two models was



**Table 2.** Parameters defining the models ( $M_1$  and  $M_2$ ) used in the preliminary analyses. For the sake of simplicity, in this table,  $\nu$  represents both  $\nu_{\text{nail}}$  (i.e., the auxetic material) and  $\nu_{\text{c-nail}}$  (i.e., a conventional material).  $\delta = 15\%$  (equation (1)) corresponds to  $R_{\text{nail}} = 15.0$  mm and  $R_{\text{cav}} = 13.0$  mm.

	$\nu$	$\alpha$	$\delta$	$E_{\text{nail}}$	$E_{\text{cav}}$
$M_1$	−0.3	100°	15%	1500 MPa	206 000 MPa
$M_2$	0.3	100°	15%	1500 MPa	206 000 MPa

used to test the hypothesis that an auxetic nail could perform better than a conventional one. Results were compared based on  $\eta$  (equation (3)).

Once the auxetic nail was compared with its conventional counterpart (i.e.,  $M_1$  vs  $M_2$ ), the goal became to explore how to increase  $\eta$  by intervening on the different parameter combinations (table 1). This allowed us to identify those influencing  $\eta$  (equation (3)) the most. The parameters  $\nu_{\text{nail}}$ ,  $\alpha$ , and  $\delta$  (equation (1)) were analyzed by varying them (based on the discretization shown in table 1) while fixing the others to their reference values. This set of simulations provided initial data on each parameter's influence on the nail-cavity system's response. However, since information on the combined effects of more than one parameter at a time was needed to deepen the nail-cavity system behavior description, a complete exploration of the design space was also performed. A different approach was developed and implemented for this part of the study.

Specifically, a surrogate model of the insertion-extraction simulations was developed to predict  $\eta$ ,  $F_{\text{ext}}$ , and  $F_{\text{ins}}$ . This approach heavily reduced the time needed to perform a parametric analysis of the system's variables. The model consisted of a regression based on a Neural Network algorithm. The algorithm was trained by providing the outputs of 6400 FE analyses related to the combination of design parameters that were investigated. All these parameter combinations were generated using the Latin hypercube sampling (LHS) method and using the parameter ranges shown in table 1.

A Python script was programmed to launch each of the 6400 simulations and extract their outputs on the Simulia/Abaqus Standard 2020 software. At the end of the simulations cycle, a database with a series of simulations correlating 6400 possible parameter combinations with their response to the insertion-extraction cycle in terms of  $F_{\text{ins}}$  and  $F_{\text{ext}}$  was created. The database generated by this process was then given as input to an Optimizable Neural Network algorithm (with 'ReLU' type activation function and size of fully connected layers equal to 283) available in the Matlab R2022a Regression Learner toolbox. Specifically, only 80% of the available data was provided to train the regression model. The objective was for the algorithm to find correlations between input parameters ( $\nu$ ,  $\alpha$ ,  $\delta$ ,  $E_{\text{nail}}$ , and  $E_{\text{cav}}$ ) and the outputs of the simulations ( $F_{\text{ins}}$ ,  $F_{\text{ext}}$ , and  $\eta$ ). The other 20% of the data was left as a testing (validation) set, which allowed us to perform an overfitting check on the algorithm. This testing set consisted of verifying that the accuracy of the regression, when applied to the testing set, was consistent with the

one exhibited during the training phase. Since the regression passed the overfitting test and exhibited relatively good accuracy (RMSE = 0.038, R-Squared = 0.84), it was sufficiently validated to be used for predicting results with new parameter combinations. These combinations differ from those employed to train the neural network. The regression model was then used to generate distributions of values describing the combined effect of two variables at a time, with the other variables fixed at specific values. Examples of such distributions will be discussed in section 3. This visual approach allowed us to explore  $\eta$  (equation (3)),  $F_{\text{ext}}$ , and  $F_{\text{ins}}$  variability more in-depth and formulate design guidelines. Comparisons between auxetic and conventional nails were also performed. The whole process is synthesized in the flowchart in figure 2.

It is worth underlying here that since the  $E_{\text{nail}}$  and  $E_{\text{cav}}$  parameters are characterized by discrete values (table 1), unlike the other parameters, which were treated as continuous variables across their ranges, the surrogate model was interrogated only on the  $E_{\text{nail}}$  and  $E_{\text{cav}}$  combinations corresponding to the ones employed in the training. This does not constitute a limitation of the study. For  $E_{\text{nail}}$  and  $E_{\text{cav}}$  values not included in the regression, dedicated simulations have been performed and compared to the results provided by the regression model. The surrogate model was used to rapidly explore the nail's design space and pinpoint possible parameter combinations that offered interesting results. Then, more detailed numerical analyses were performed to evaluate and quantify the nail's behavior.

### 3. Results and discussion

Results show that the auxetic insert proves to be a better solution than a conventional one. Besides, the methodology developed and implemented to deepen the parameters' influence has been fruitful for elaborating design guidelines. In this section, first, the results obtained from the preliminary FEM analyses are discussed (section 3.1), followed by a detailed description of these guidelines (section 3.2).

#### 3.1. Results of the preliminary analyses and parameter sensitivity study

The main outputs of the  $M_1$  model (table 2) are summarized in table 3. Values of  $F_{\text{ins}}$  and  $F_{\text{ext}}$  are the peaks of the output plot like the one shown in figure 3.

The three analysis steps described in section 2.2, take a total time of eight time units (figure 3). It should be observed that in this quasi static analysis time has only the role of ordering the events originated by the applications of the boundary conditions referred to each step. Although figure 3 refers only to a specific design, it is worth anticipating that this peak trend will be the same for all the simulations.

$F_{\text{ins}}$  is much higher in value (145 118 N) than  $F_{\text{ext}}$  (6179 N), as reflected by the low  $\eta$  (0.043). This means that such geometry opposes a high resistance to being pushed into the cavity more than it does to being pulled out. It is worth highlighting that both forces have high values. From a practical

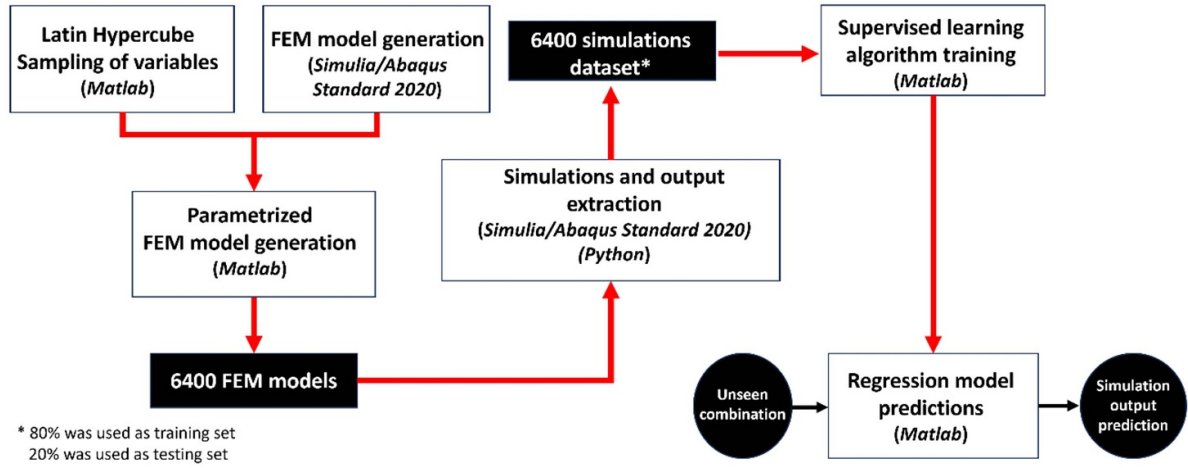


**Figure 2.** Flowchart of the regression model generation process. A 6400 FE simulation outputs database was generated with the Simulia/Abaqus Standard 2020 software on models defined by parameter combinations obtained by applying a Latin Hypercube Sampling (LHS) on the parameter ranges introduced in table 1. The database was used to train a supervised learning algorithm to produce a regression model used as a surrogate for new FE simulations run on previously unseen parameter combinations.

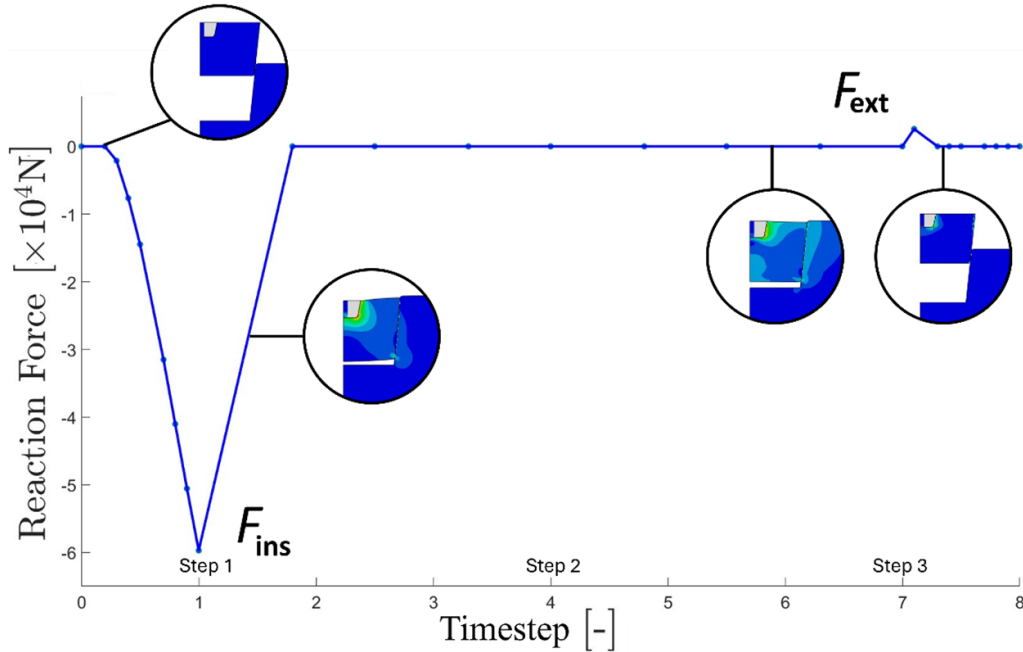


**Figure 3.** Results of an example of auxetic nail simulation: evolution of the reaction force acting on RP during the timesteps and corresponding frames of the simulations (Von Mises stress contours are shown). Further details on the insertion and extraction cycle steps are provided in section S1.4 of the supporting information.

point of view, it would not be easy to extract this type of nail. It is important to note that the boundary conditions were changed after the complete insertion of the nail, which was carried out by imposing a displacement on it. The nail was left free to allow a possible ejection of the nail from the cavity, which never happened. At a high  $\eta$  rate (equation (3)), the comparison with its conventional counterpart, through the  $M_2$  model (table 2), has highlighted its potential superior capabilities demonstrated by its higher  $\eta$  value (table 3).

Figures 4–6 instead show the results of the second preliminary study focused on exploring how  $\eta$  is influenced by  $\nu_{\text{nail}}$ ,  $\delta$  (equation (1)), and  $\alpha$ .

**Table 3.** Outputs of the simulations run on the  $M_1$  and  $M_2$  (table 2) preliminary models.

	$F_{\text{ins}}$ (N)	$F_{\text{ext}}$ (N)	$\eta$ (–)
$M_1$	145 118	6179	0.043
$M_2$	245 257	4466	0.018

The parameter with the most complex relationship with  $\eta$  was found to be  $\nu_{\text{nail}}$ . The distribution has no clear trend as  $\eta$  values fluctuate while  $\nu_{\text{nail}}$  gets increasingly negative. The  $\nu_{\text{nail}}$  influence on the absolute value of the force is even more

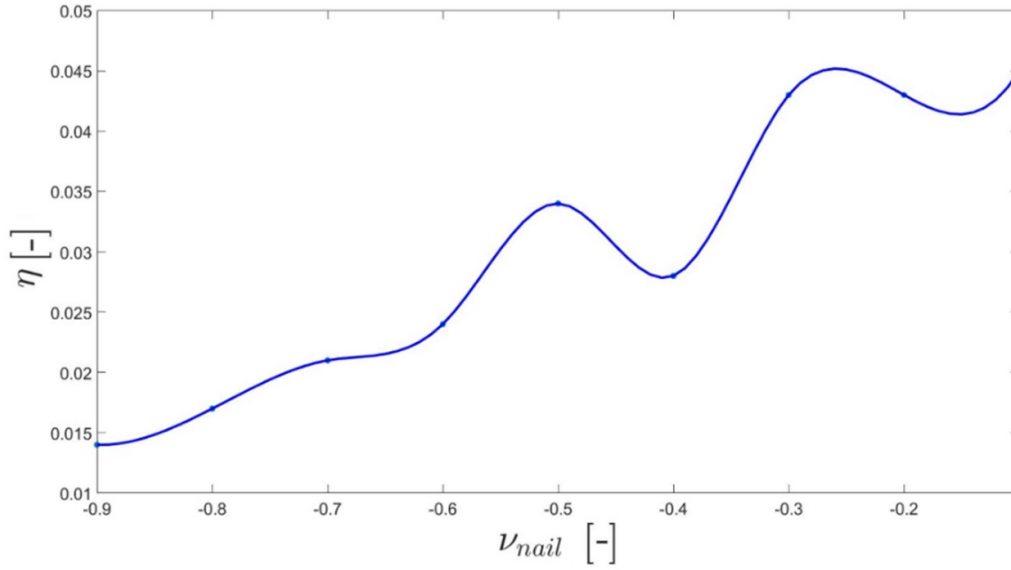


**Figure 4.** Distribution of  $\eta$  (equation (3)) values with respect to  $\nu_{\text{nail}}$  ( $\alpha = 100^\circ$ ,  $R_{\text{nail}} = 15$  mm,  $E_{\text{nail}} = 1500$  MPa,  $E_{\text{cav}} = 206\,000$  MPa).

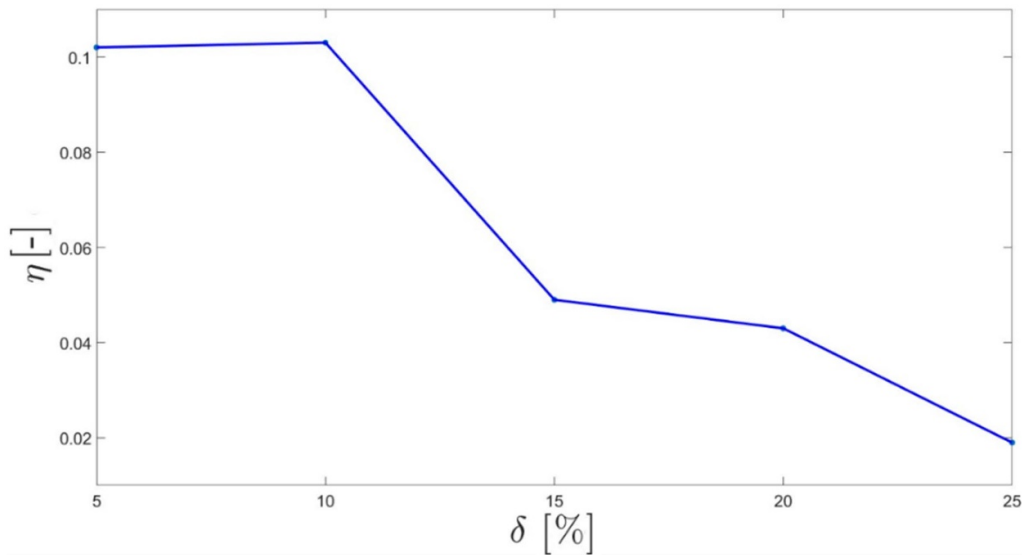


**Figure 5.** Distribution of  $\eta$  (equation (3)) values with respect to  $\delta$  ( $\nu_{\text{nail}} = -0.3$ ,  $\alpha = 100^\circ$ ,  $E_{\text{nail}} = 1500$  MPa,  $E_{\text{cav}} = 206\,000$  MPa).

irregular and unclear (figure 7). The distributions of  $\eta$  with respect to  $\delta$  (figure 5) and  $\alpha$  (figure 6) shift to higher values as the two parameters decrease. Therefore, the influence that  $\nu_{\text{nail}}$ ,  $\alpha$ , and  $\delta$  have on  $\eta$  did not prove to be sufficient to increase  $\eta$  by a significant amount.

These results demonstrated that a much more comprehensive study was necessary to understand the maximum values the nail-cavity system can reach through an optimal combination of these parameters.

### 3.2. Surrogate model and nail-cavity design guidelines

The results obtained from the surrogate model are presented as design guidelines. In total, three design guidelines were elaborated. Each indicates the main principles to be followed when

making a design choice. Sometimes, they may refer to specific situations; in other cases, they are intended more as general rules.

**3.2.1. Superior performance of a nearly cylindrical nail in the presence of a rigid cavity.** This finding is presented as the first because it is the most evident trend from the analysis. Indeed, the distribution of  $\eta$  as a function of  $\alpha$  and  $\nu_{\text{nail}}$ , shown in figure 8, clearly indicates that when dealing with a cavity in a rigid material (e.g., steel:  $E \sim 206\,000$  MPa, low  $\gamma$ , see equation (2)), simulations suggest using a cylindrical nail ( $\alpha = 90^\circ$ ).

As shown in figure 8, even when the overall distribution may have a complex shape, with some peaks and valleys in specific areas, it is quite clear that there is a strong inverse



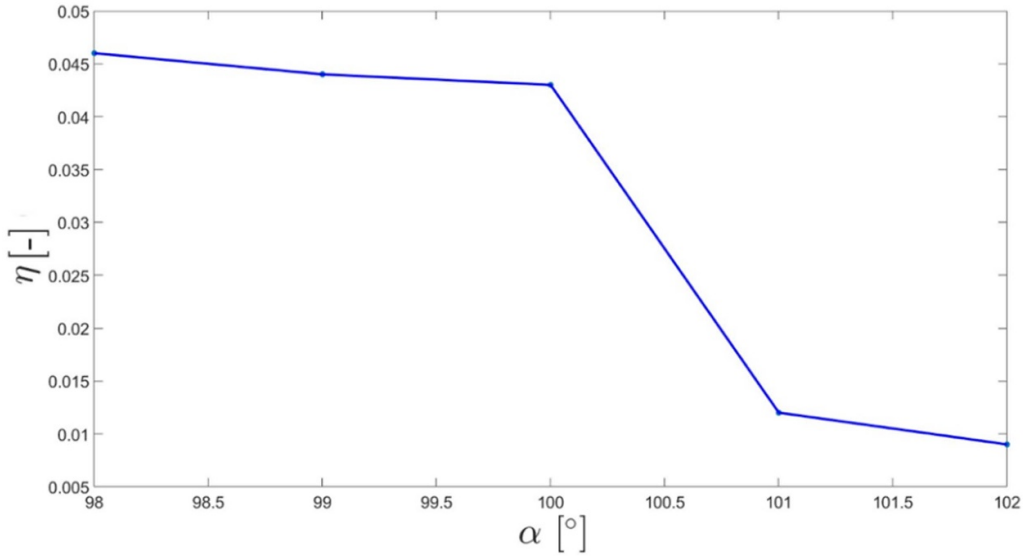


**Figure 6.** Distribution of  $\eta$  (equation (3)) values with respect to  $\alpha$  ( $\nu_{\text{nail}} = -0.3$ ,  $R_{\text{nail}} = 15$  mm,  $E_{\text{nail}} = 1500$  MPa,  $E_{\text{cav}} = 206\,000$  MPa).

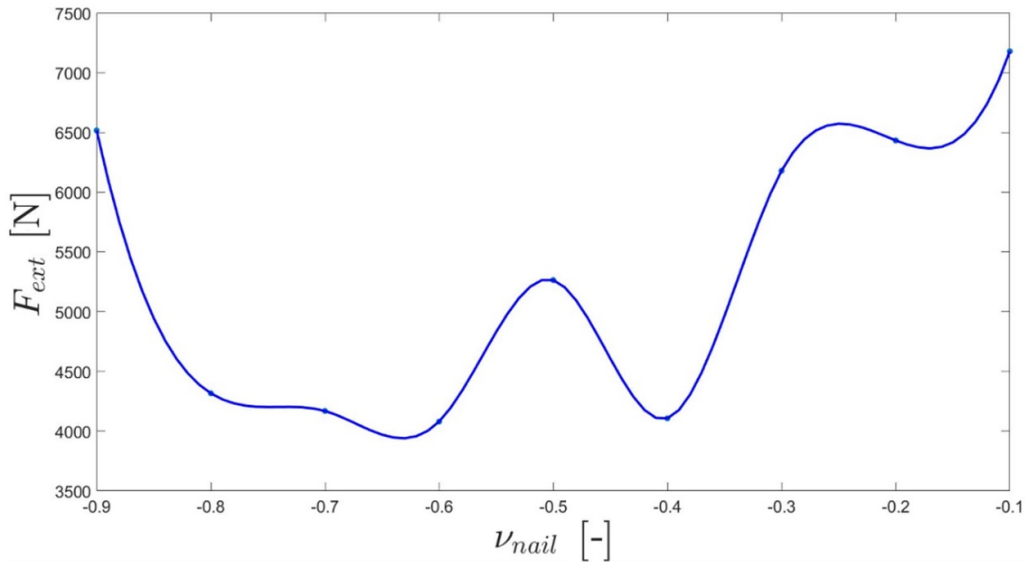


**Figure 7.** Distribution of values with respect to  $\nu_{\text{nail}}$ , with  $\alpha = 100^\circ$ ,  $R_{\text{nail}} = 15$  mm,  $E_{\text{nail}} = 1500$  MPa, and  $E_{\text{cav}} = 206\,000$  MPa.

correlation between  $\alpha$  and  $\eta$ : the highest efficiencies are found for  $\alpha \rightarrow 90^\circ$ .

Distributions of  $\eta$  with respect to  $R_{\text{nail}}$  were also studied. They shared the same  $\eta$ - $\alpha$  correlation. A few examples are reported in the Supporting Information (section S2).

To understand better the role of  $\alpha$ , simulations considering specific parameter combinations were run. The results are consistent with those from the regression model and provide further useful information. They are shown in table 4. They confirm the overall trend of the distribution in figure 8:  $\alpha$  closer to  $90^\circ$  led to an increase in the efficiency values ( $\eta$ , equation (3)).

The  $\alpha$  parameter has a key influence on the forces the nail has to deal with. Though, as explained later in section 3.2.2, the material and nail-cavity interference design are the two most important steps to operate with forces compatible with

the nail's field of application. Hence, a proper material/structure (i.e.,  $E_{\text{nail}}$ ) selection sets us on the desired order of magnitude. Still, a proper  $\alpha$  can avoid the issue of dealing with insertion pressures that are not manageable.

It is worth highlighting that optimal  $\alpha$  values allow increasing  $\eta$  by acting positively on both terms of the ratio (they lower  $F_{\text{ins}}$  and increase  $F_{\text{ext}}$ , see also equation (3)). This is quite unusual since, as we will see, parameters often act similarly on both forces (by simultaneously increasing or decreasing them).

This information also provides an interesting insight into the working mechanism of the auxetic nail. It is expected that the compression exerted during the insertion helped shrink the nail so that it could have been inserted into a conical cavity with lower forces (lower  $F_{\text{ins}}$ ). At the same time, the tension exerted during the pull-out process would have expanded the

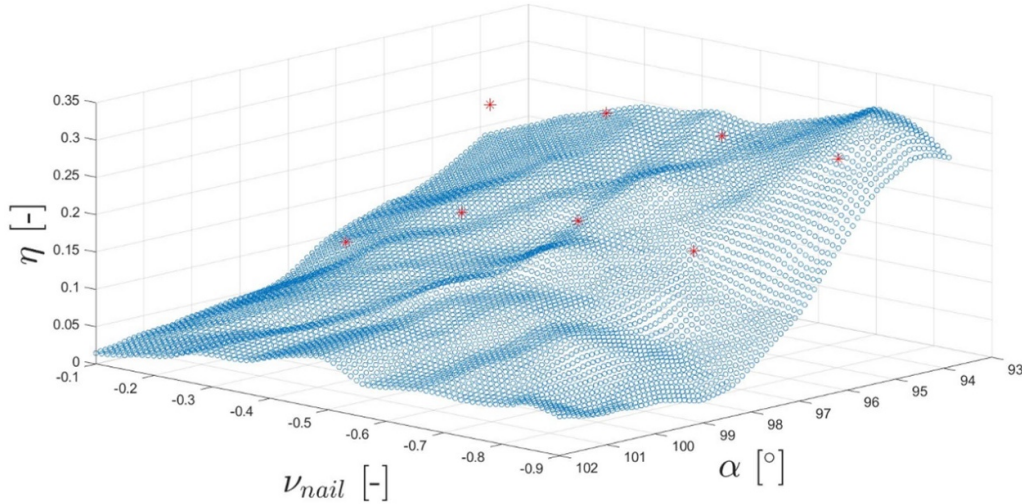


**Figure 8.** Distribution of  $\eta$  (i.e., the efficiency parameter) values with respect to  $\nu_{\text{nail}}$  and  $\alpha$  obtained thanks to the regression model (red stars show the results of simulations that were run to verify the regression model trend prediction). The following values were assigned to the other parameters:  $R_{\text{nail}} = 14$  mm,  $E_{\text{nail}} = 1500$  MPa,  $E_{\text{cav}} = 206\,000$  MPa.

**Table 4.** Results provided by the Simulia/Abaqus Standard 2020 non-linear simulations. They were run on models defined by the following parameters:  $\nu_{\text{cav}} = 0.9$ ,  $\delta = 3.8\%$ ,  $E_{\text{nail}} = 250$  MPa,  $E_{\text{cav}} = 206\,000$  MPa. A lower  $\alpha$  value reduces  $F_{\text{ins}}$  while it increases  $F_{\text{ext}}$ . Therefore, at a lower  $\alpha$  angle,  $\eta$  reaches its highest value. These changes are also highlighted using percentages.

$\alpha$	$F_{\text{ins}}$ (N)	$F_{\text{ext}}$ (N)	$\eta$ (—)
98°	3969	651	0.16
92°	2905	1255	0.43
	−27%	+193%	+268%

nail, thus hindering the extraction (higher  $F_{\text{ext}}$ ). Simulations represented by red stars in figure 8 show that auxeticity reduces the force values. Still, it does not affect the fact that a cylindrical cavity is more suited to increase  $\eta$  than a tapered one.

Comparing an auxetic nail with its conventional counterpart ( $\nu_{\text{c-nail}} = 0.4$ ) using the better performing model among those studied (i.e.,  $\alpha = 92^\circ$ ,  $R_{\text{nail}} = 15$  mm,  $E_{\text{nail}} = 1500$  MPa,  $E_{\text{cav}} = 206\,000$  MPa) we obtained again that the auxetic nail (figure 9(a)) fit more easily in its cavity. Figure 9 shows the von Mises stress distribution of the two nails once fully inserted. Once the auxetic nail has been completely pushed in, the distortion from the original shape is lower than that of the corresponding conventional nail (figure 9(b)), thanks to its ability to shrink along both principal directions. As the stress distributions suggest, the auxetic nail is more ‘relaxed’. Stresses are about one order of magnitude lower than in the conventional counterpart. This aspect may be even more stressed for different friction coefficients, which, as already mentioned, were neglected in this parametric analysis.

Reaction forces obtained as outputs from the simulations are shown in table 5. Auxetic nails lower dramatically the pressure that needs to be applied to push them in and lower the force needed to pull them out of the cavity. The efficiency of an auxetic nail lies in the fact that it performs better if the overall

pull-in-and-out process is considered, but it does not hinder its extraction. The results point out that the ability of auxetics to adapt to cavities is the main feature that led them to be the best solution. Their ability to expand horizontally when pulled vertically is almost irrelevant, unlike what could be expected, as that capability is one of the distinguishing features of auxetic materials.

As introduced at the beginning of this Section, the positive effect of cylindrical cavities on  $\eta$  values can be witnessed when  $E_{\text{cav}} > E_{\text{nail}}$  (i.e.,  $\gamma \rightarrow 0$ , see equation (2)). Figure 10 shows an example of a parameter combination where  $\gamma = 6$  (i.e.,  $E_{\text{nail}} = 1500$  MPa,  $E_{\text{cav}} = 250$  MPa, see also equation (2)). The distribution shows that the correlation between  $\alpha$  and  $\eta$  cannot be synthesized by the guidelines presented in this section. Indeed, the case presented in figure 10 shows a clear  $\eta$  reduction when  $\alpha$  approaches values close to  $90^\circ$ . Therefore, further guidelines were elaborated.

**3.2.2. Influence of the nail-cavity interference  $\delta$  on the absolute magnitude of  $F_{\text{ins}}$  and  $F_{\text{ext}}$ .** The analysis of the effects of the parameter  $\delta$  (equation (1)) on the nail-cavity system highlights another evident trend. As shown in figure 11, the combined effect of  $\alpha$  and  $R_{\text{nail}}$  generates curves that generally exhibit maxima for low  $R_{\text{nail}}$  values (i.e., with relatively low interference between the nail and the cavity since  $R_{\text{cav}}$  was kept fixed at 13.0 mm). Additional distributions have also been generated considering different values of  $\gamma$  (i.e., different material combinations). Figures 12 and 13 show two examples. In both cases, the results obtained were similar and indicate that, for each case, the efficiency (i.e.,  $\eta$ ) can be maximized through a proper choice of that interference.

However, although each combination of parameters led to different maxima for  $\eta$ , a close analysis can identify that the optimal value of  $R_{\text{nail}}$  to maximize the efficiency is 13.6 mm, corresponding to an interference  $\delta = 4.6\%$  (see equation (1)).

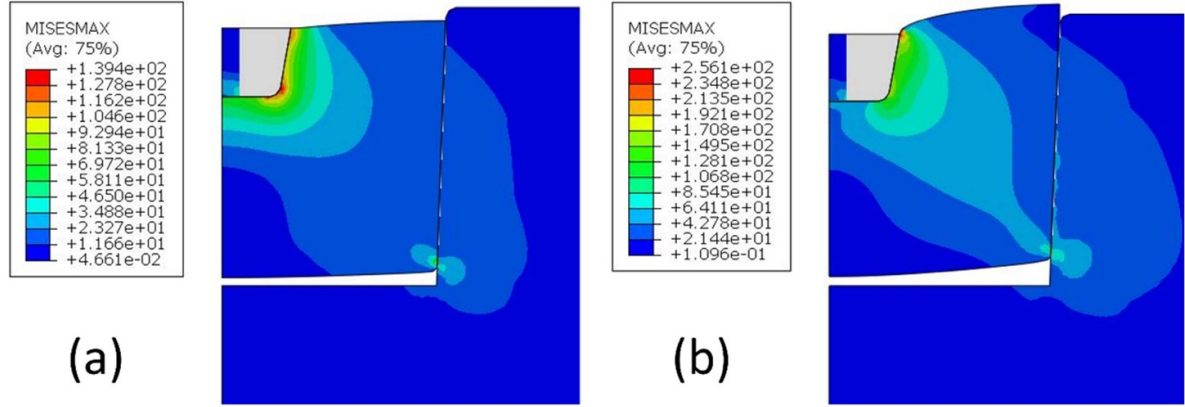


**Figure 9.** Von Mises stress distribution (MPa) in (a) an auxetic and (b) a conventional nail. The models are based on:  $\alpha = 92^\circ$ ,  $\delta = 3.8\%$ ,  $E_{\text{nail}} = 250$  MPa,  $E_{\text{cav}} = 206\,000$  MPa.

**Table 5.** Results provided by Simulia/Abaqus Standard 2020 non-linear simulations ran on models with  $\alpha = 92^\circ$ ,  $\delta = 3.8\%$ ,  $E_{\text{nail}} = 250$  MPa,  $E_{\text{cav}} = 206\,000$  MPa.

	Auxetic ( $\nu_{\text{nail}} = -0.4$ )	Conventional ( $\nu_{\text{c-nail}} = 0.4$ )
$F_{\text{ins}}$ (N)	2905	83 426
$F_{\text{ext}}$ (N)	1255	2043
$\eta$ (—)	0.43	0.24

Even though each combination of parameters led to different peak heights and  $\eta$  values, the peak's type and position remained almost constant.  $\delta$  (i.e., the interference between the nail and the cavity, equation (1)) values around 3.8% appear to be the best design option. Moreover, it is important to remember that  $\alpha$  and  $R_{\text{nail}}$  are strictly related by the geometrical condition discussed in section 2. Lower  $R_{\text{nail}}$  values allow designing nails with a lower  $\alpha$ .

As previously demonstrated, nearly cylindrical shapes are an ideal solution. Therefore, a relatively low interference design is the best option if it is high enough to compress the nail and exploit its auxeticity. Nevertheless, from a practical point of view, being the best solution does not mean that the  $\eta$  values they provide are always significantly higher. The performance increase can often become almost negligible depending on the materials employed. Despite being more efficient, low-interference couplings may not always be the best option. This is because of the huge impact that  $\delta$  has on the forces to be provided to pull the nail in and out of the cavity.

Figure 14 shows the typical distribution of  $F_{\text{ins}}$  depending on  $R_{\text{nail}}$  and  $\alpha$ . Even a small  $R_{\text{nail}}$  rise significantly increases the force to insert the nail into the cavity.

This result is important because it allows tuning the nail-cavity system for specific purposes. For example, let us assume we need a nail that is hard to pull out. We could choose to operate under large interference conditions, being aware that we should be able to provide the necessary force to push the nail in. A conventional nail would struggle to stay put in this interference condition. On the contrary, an auxetic nail, since it can

undergo a large compression in both principal directions, can stabilize its position in the cavity. Figure 15 explains the difference between these two nails. Although both can be inserted into the cavity, the auxetic nail (figure 15(a)) perfectly fits it. In contrast, the conventional one (figure 15(b)) is not in equilibrium condition and tries to escape from the cavity. The higher the interference, the more relevant the difference between these two behaviors is. This aspect can be particularly relevant in specific practical applications. For example, in biomedical applications (e.g., tooth implants), empty cavities could prove to be highly determinantal and become a site for bacterial growth that leads to infection. Similarly, in applications where products are in contact with water, such as in water-sports applications (e.g., components of rowing oars), cavities could lead to water ingress, leading to faster deterioration.

However, for the complete tuning of the forces, other aspects must be controlled (we previously mentioned the relevance of  $\alpha$  in this field), and many of them are challenging to synthesize through a design rule. Materials and friction are just two examples of the model's features that should be introduced, studied, and designed for this purpose. Interference selection is just the first step of this force-tuning process.

**3.2.3. Auxetic nail efficiency depends on the material of the cavity.** The influence of  $\nu_{\text{nail}}$  in the performance of the auxetic nail is strictly related to the material of the cavity. Since auxeticity is a property acting on the deformation mechanism, its impact on the material's behavior depends on the amount of deformation applied.

Let us assume that a soft material is selected to fill a very rigid cavity (e.g., steel-like cavity:  $E_{\text{cav}} = 206\,000$  MPa,  $\gamma \rightarrow 0$ , equation (2)) with a small  $R_{\text{cav}}$  ( $\delta \uparrow$ ). Hence, a large deformation must be applied to insert the nail. As we have seen, auxeticity can significantly contribute to this situation because it helps the material to adapt to the cavity. Instead, if the cavity is manufactured using a soft material (e.g.,  $E_{\text{cav}} = 250$  MPa,

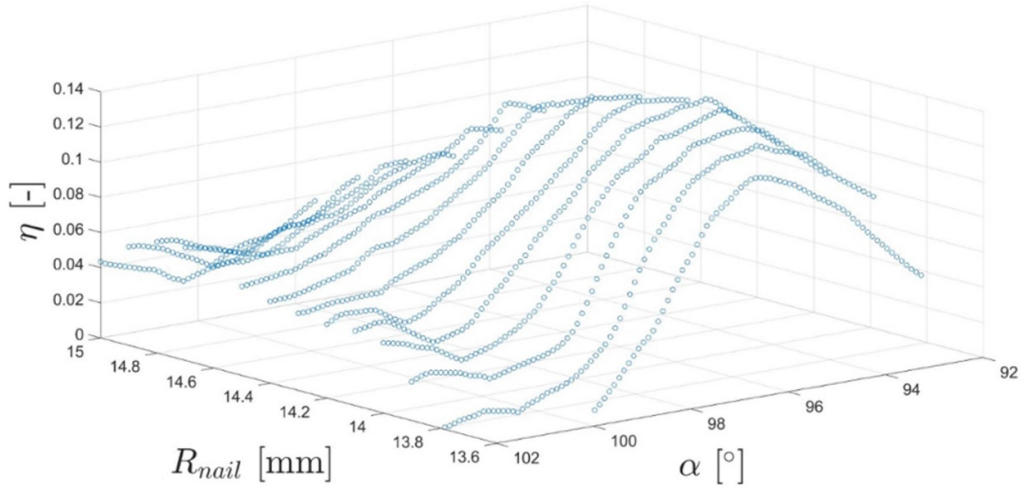


**Figure 10.** Distribution of  $\eta$  values with respect to  $R_{\text{nail}}$  and  $\alpha$  with  $\nu_{\text{nail}} = -0.4$ ,  $E_{\text{nail}} = 1500$  MPa, and  $E_{\text{cav}} = 250$  MPa.

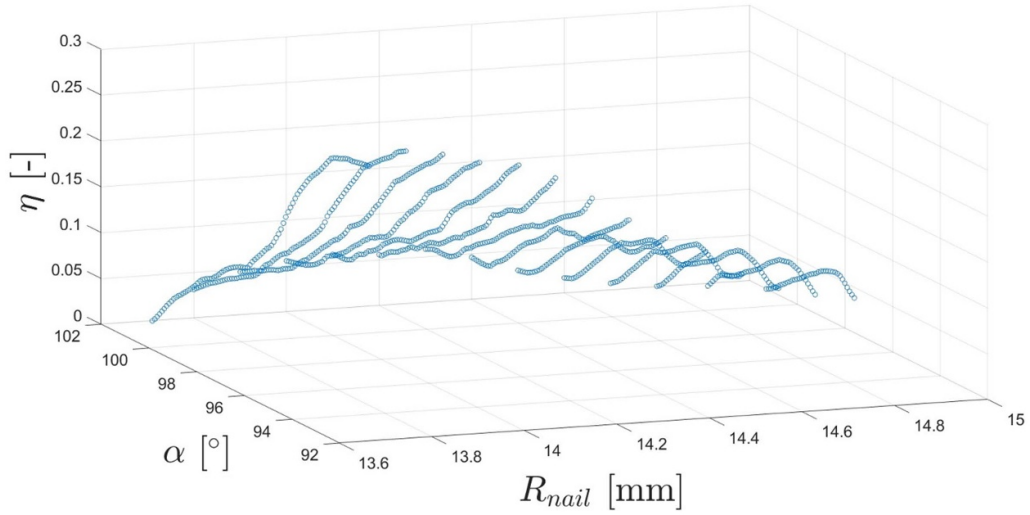


**Figure 11.** Distribution of  $\eta$  (equation (3)) values with respect to  $R_{\text{nail}}$  and  $\alpha$  with  $\nu_{\text{nail}} = -0.4$ ,  $E_{\text{nail}} = 250$  MPa, and  $E_{\text{cav}} = 206\,000$  MPa.

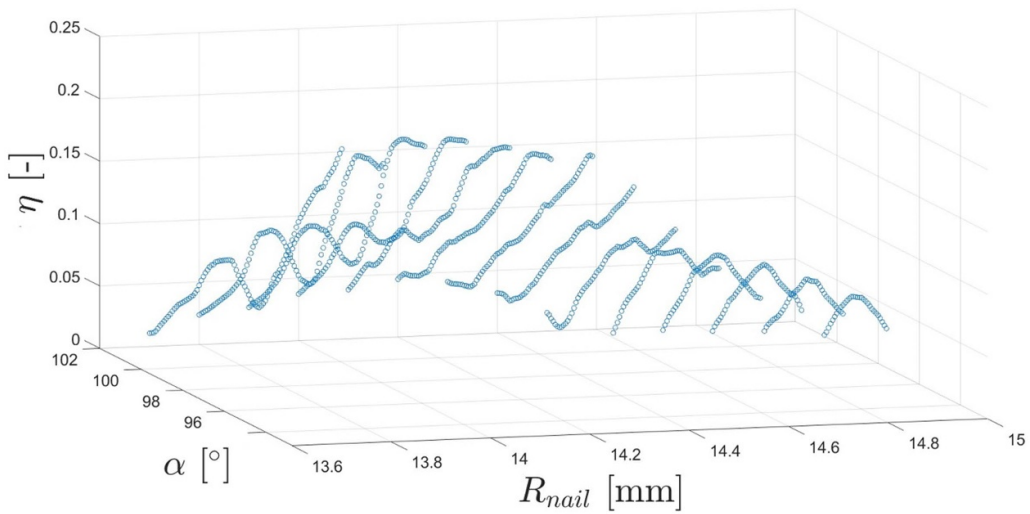


**Figure 12.** Distribution of  $\eta$  (equation (3)) values with respect to  $R_{\text{nail}}$  and  $\alpha$  with  $\nu_{\text{nail}} = -0.4$ ,  $E_{\text{nail}} = 750$  MPa, and  $E_{\text{cav}} = 1500$  MPa.



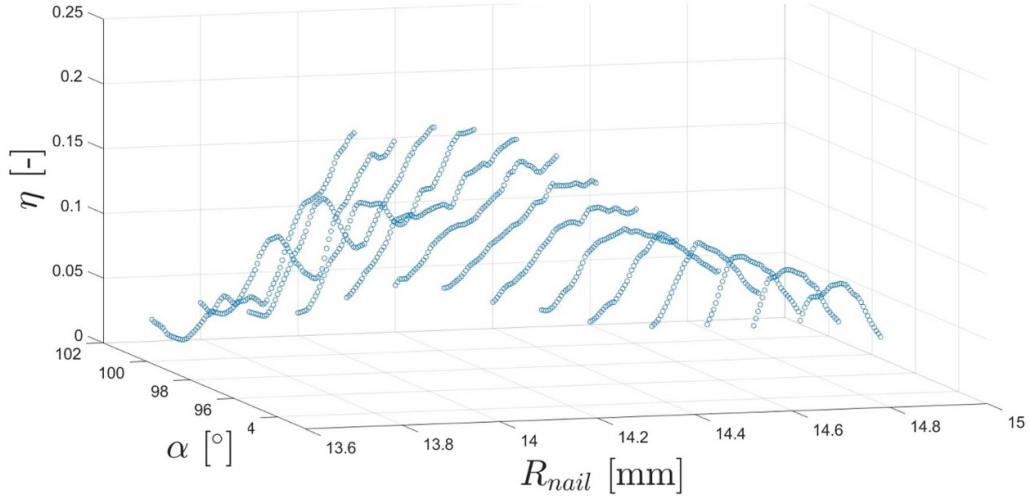


**Figure 13.** Distribution of  $\eta$  (equation (3)) values with respect to  $R_{\text{nail}}$  and  $\alpha$  with  $\nu_{\text{nail}} = -0.4$ ,  $E_{\text{nail}} = 750$  MPa, and  $E_{\text{cav}} = 750$  MPa.

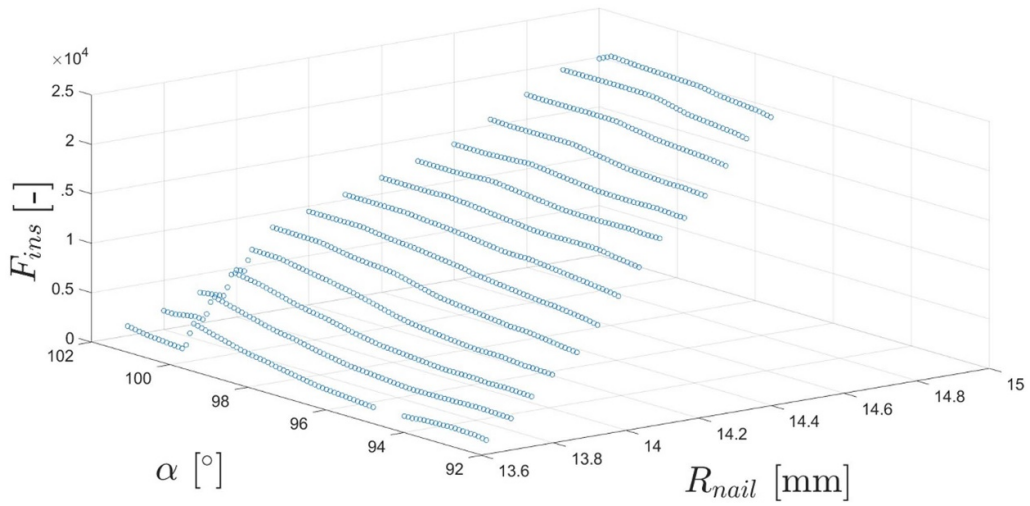


**Figure 14.** Distribution of  $F_{\text{ins}}$  with respect to  $R_{\text{nail}}$  and  $\alpha$  with  $\nu_{\text{nail}} = -0.4$ ,  $E_{\text{nail}} = 250$  MPa, and  $E_{\text{cav}} = 206\,000$  MPa.

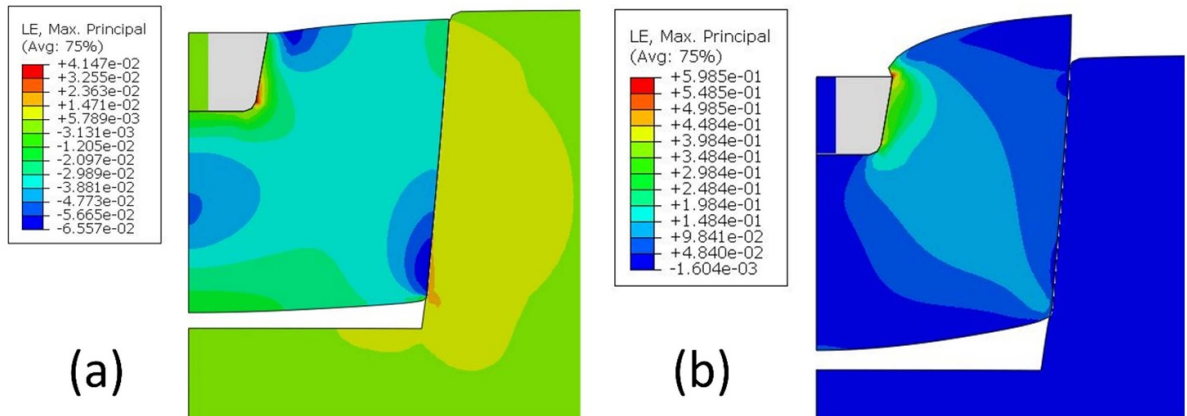


**Figure 15.** Von Mises stress distribution in (a) an auxetic ( $\nu_{\text{nail}} = -0.4$ ) and (b) a conventional nail ( $\nu_{\text{c-nail}} = 0.4$ ). The models are based on:  $\alpha = 95^\circ$ ,  $\delta = 7.6\%$ ,  $E_{\text{nail}} = 250$  MPa,  $E_{\text{cav}} = 750$  MPa.



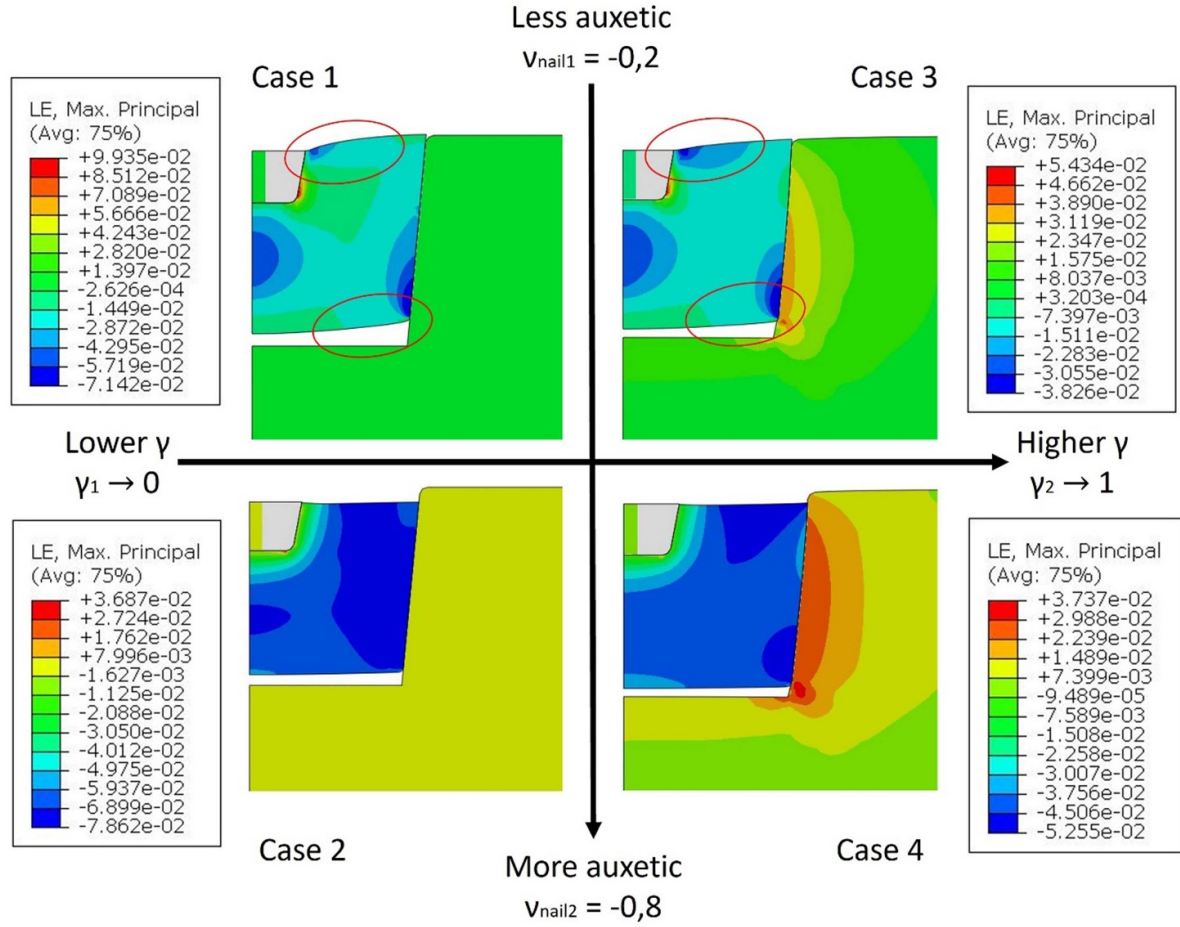


**Figure 16.** Comparison of the different Maximum Principal Logarithmic Elastic Strain (LE) contours generated by models differing because of  $\nu_{\text{nail}}$  and  $E$  values ( $|\nu_{\text{nail}1}| < |\nu_{\text{nail}2}|$  and  $\gamma_1 < \gamma_2$ ).

$\gamma \sim 1$ ), pressure on its walls would be enough to make it undergo deformation, reducing the level of distortion applied to the nail. In this case, auxeticity is still useful but less needed because the cavity has deformed to fit the nail much better. Hence, the influence of  $\nu_{\text{nail}}$  depends on the materials the nail must deal with.

Figure 16 shows the results of four simulations run on different models to explain that phenomenon. Maximum Principal Logarithmic Elastic Strain (LE in Simulia/Abaqus Standard 2020 settings) was picked as the output. It is shown as a color contour according to the legends reported in the images. The frames in figure 16 correspond to the moment the nail has just been completely pushed in.

In the application hypothesis considered in figure 16, two possibilities were set for the  $\nu_{\text{nail}}$  value:  $\nu_1 = -0.2$  and  $\nu_2 = -0.8$ . They represent a low and a highly auxetic material, respectively. For the elastic modulus of the nail and the cavity, the following choices were made:

- (1)  $\gamma_1 \rightarrow 0$ :  $E_{\text{nail}1} = 250 \text{ MPa}$  and  $E_{\text{cav}1} = 206000 \text{ MPa}$ ;
- (2)  $\gamma_2 \rightarrow 0$ :  $E_{\text{nail}2} = 750 \text{ MPa}$  and  $E_{\text{cav}2} = 750 \text{ MPa}$ .

The first choice represents the situation where a soft nail is selected to fill a rigid cavity. In contrast, the latter represents the case where the nail and the cavity walls are equally rigid

and have the same Young modulus. The four studied models result from all the possible combinations of these  $\nu_{\text{nail}}$  and  $\gamma$  values.

We will first analyze the simulation resulting in the frame shown in the upper-left corner of figure 16 (Case 1). It is based on the  $\nu_{\text{nail}1} - \gamma_1$  combination, which generates a scarcely auxetic nail and a very rigid cavity. Even though the auxetic nature of the nail has helped it enter the cavity, its shape has been distorted to get in fully. The top and bottom surfaces are the parts of the nail that show this aspect more evidently. Moving to the top-right part of figure 16 (Case 3), we are now looking at the simulation resulting from the  $\nu_{\text{nail}1} - \gamma_2$  combination. In this case, a low negative  $\nu_{\text{nail}}$  nail has entered a cavity softer than the one in the previous case ( $E_{\text{cav}2} < E_{\text{cav}1}$ ), whose walls have thus helped the insertion process. This consideration comes from the more regular deformed shape and the more uniform distribution of the LE values. The curvature of the top and bottom surfaces of the nails can be used as an indicator, as it is lower than in the previous case (Case 1). Such results prove that a lower Poisson in magnitude (i.e., a less auxetic structure/material) can have very different effects according to the elastic modulus of the nail's and cavity's materials.

**Table 6.** Outputs of the non-linear simulations with  $E_{\text{nail}} = 750$  MPa,  $E_{\text{cav}} = 750$  MPa. The percentage indicates the  $F_{\text{ins}}$  reduction obtained with an increase of the absolute value of  $\nu_{\text{nail}}$ .

$\nu_{\text{nail}} (-)$	$F_{\text{ins}} (\text{N})$
-0.2	13 199
-0.6	11 559
	-12%

**Table 7.** Outputs of the non-linear simulations with  $E_{\text{nail}} = 250$  MPa,  $E_{\text{cav}} = 206\,000$  MPa. The percentage indicates the  $F_{\text{ins}}$  reduction obtained with an increase of the absolute value of  $\nu_{\text{nail}}$ .

$\nu_{\text{nail}} (-)$	$F_{\text{ins}} (\text{N})$
-0.2	7218
-0.6	5778
	-20%

Case 2 at the bottom-left position in figure 16 shows the simulation obtained by the combination  $\nu_{\text{nail}2} - \gamma_1$ . In this case, a highly auxetic nail has entered a rigid cavity. Compared to Case 1, the curvature of the nail surfaces demonstrates that the nail has entered the cavity more easily because it has not been distorted too much from the original shape (as highlighted by the red circles). LE distribution is much more homogeneous and has lower values, confirming that the negative  $\nu_{\text{nail}}$  value has helped uniformly shrink the nail during insertion. This auxetic nail performs much better than the less auxetic one (Case 1) when used to fill a rigid cavity.

Finally, Case 4 in figure 16 shows the results of the  $\nu_2 - \gamma_2$  combination. As expected, this is the most efficient combination, as highlighted by the distortion that ends up being applied to the nail. Contours show a uniform LE distribution, with the lowest LE values obtained so far; the top and bottom surfaces are not curved that much. The original overall shape of the nail has not been significantly distorted; it simply shrunk along both principal directions.

Comparing the frames on the bottom of figure 16 (Cases 2 and 4) with the ones on the top (respectively, Cases 1 and 3), we can notice that the two images on the left (Cases 1 and 2) exhibit very significant changes, while the ones on the right (Cases 3 and 4) look more similar. This means that increasing the degree of auxeticity in the case of a rigid cavity has had a larger impact than in the case of a soft one. Extending this result to situations where cavities are in highly soft materials, we can conclude that designing a nail with highly negative  $\nu$  when the cavity can adjust to its presence may not be that beneficial.

Finally, tables 6 and 7 show the outputs of the simulations to quantify the improvement that shifting from a  $\nu_{\text{nail}} = -0.2$  to a  $\nu_{\text{nail}} = -0.6$  may provide depending on the materials. The parameter used as a reference for the evaluation is the force needed to push the nail in. The trend is that cavities in rigid materials leave more room for improvement in  $F_{\text{ins}}$  reduction (i.e., -20% vs -12%, tables 6 and 7) if  $\nu_{\text{nail}}$  is increased in modulus (e.g.,  $\nu_{\text{nail}} \rightarrow -0.9$ ).

#### 4. Final considerations and conclusion

This study aimed to establish the basis for investigations that exploit the auxetic behavior in specific operational conditions. Indeed, despite the numerous studies and the manufacturing opportunities available, the use of auxetics for structural applications has not gone as far as one could expect due to the lack of general design guidelines to drive forward the exploitation of real-world applications of auxetic materials.

To deal with this issue, in this study a model based on homogenized auxetic isotropic materials was used to investigate how and in which cases auxetic materials or structures could represent a more effective solution than conventional materials. A numerical approach was chosen to avoid the influence of topological and practical aspects (such as fabrication defects) that could have distorted the result. A nail-cavity system was considered the design domain to be explored, where the nail is built using a bulk auxetic material and the cavity a conventional one. Relevant design parameters for this system have been identified, and their influence on the system's behavior has been explored. A surrogate model was also created using a supervised learning algorithm to predict the outcomes of each parameter combination. The following findings and considerations have been elaborated:

- An almost cylindrical nail is the best-performing solution for filling a rigid cavity (e.g., steel-like material  $E = 206\,000$  MPa).
- The ‘mechanical interference’ between the nail and the cavity is the most relevant aspect to finely tuning  $F_{\text{ins}}$  and  $F_{\text{ext}}$ .
- The effect of auxetic behavior on the performance of the nail depends on the material of the cavity.

Concerning the first finding, results demonstrate that  $\eta$  values can be more than doubled if  $\alpha$  is close to  $90^\circ$ . From a design point of view, this may result in a useful strategy as controlling  $\alpha$ , unlike other parameter selection, allows decreasing  $F_{\text{ins}}$  and increasing  $F_{\text{ext}}$  simultaneously.

Concerning the second consideration, the results have demonstrated that changing  $R_{\text{nail}}$  values in the 13.6 mm–15 mm range ( $\delta = 3.8\%–25\%$ ) may lead to an order of magnitude shift for  $F_{\text{ins}}$  and  $F_{\text{ext}}$ . At the same time, varying  $R_{\text{nail}}$  in that range only accounts for a small  $\eta$  change (values barely witness a 0.1–0.2 variation), making  $R_{\text{nail}}$  almost irrelevant for an ‘efficiency’ optimization. Therefore,  $R_{\text{nail}}$  is much more effective in defining the order of magnitude of the force values than finding the optimal design solution for optimization purposes.

Finally, the third consideration is used to underlying that when dealing with a steel-like cavity ( $E = 206\,000$  MPa), auxetic nails (which are most likely to have polymer-like elastic moduli,  $E = 19$  MPa–1500 MPa) perform at their best by appreciably reducing the intensity of the force needed for the nail insertion than conventional materials ( $F_{\text{ins}} \approx 20\%$  decrease). Auxetic nails settle in the cavity with relative ease, unlike conventional nails. On the other hand, if the

nail and the cavity have elastic moduli with similar values (e.g., polymeric nail-polymeric cavity system), improvement granted by an auxetic nail compared to a conventional one is lower ( $F_{\text{ins}} \approx 10\%$  decrease). Cavity walls and the nail will deform to favor the insertion. This will happen with both the auxetic and conventional nails.

In general, the negative Poisson's ratio of auxetic nails improves their ability to enter the cavity. It limits their tendency to exit when the pushing action ends, leaving them free to move. Moreover, despite  $F_{\text{ext}}$  never reaching values larger than  $F_{\text{ins}}$ ,  $\eta$  can still be maximized by operating on specific parameters depending on geometric and material factors.

The various steps of this process can be further improved by adding new factors, such as friction or additional geometric parameters influencing the nail shape, to the analysis to make the description of the auxetic behavior more accurate. However, since the relative motion between the two bodies is significant compared to their dimensions, modeling friction effects when the coefficient is high may cause large element distortion. Increased computational power would be, therefore, needed.

The model can also be modified to consider more complex technical solutions. Different  $\nu_{\text{nail}}$  values could be attributed to distinct 'subdomains' or 'zones' of the nail. The overall deformation of the nail should be affected by this design choice, influencing the insertion and extraction from the cavity. The developed approach can also be exploited to find the optimal solution for a specific design case, with well-defined strength values required by the junction, maximizing the ratio between the extraction and the insertion forces.

Finally, for a pragmatical finalization of this work, it is paramount to explore how to physically render the auxetic component, i.e., how to design and fabricate it, exploiting the design potential offered by AM technologies. Nowadays, there are multiple ways of obtaining 3D auxetic structures, from periodic cellular structures to novel origami-based designs and foams [35, 47, 56, 57]. Therefore, the current knowledge of auxetic structures, combined with the design guidelines derived through our study, can allow the development of effective fasteners for various applications.

## Data availability statement

The data cannot be made publicly available upon publication because they are not available in a format that is sufficiently accessible or reusable by other researchers. The data that support the findings of this study are available upon reasonable request from the authors.

## Acknowledgments

J N G gratefully acknowledges the support of the University of Malta Research Fund and that of the Malta Council for Science & Technology. Part of this work was financed by the Malta Council for Science & Technology, for and on behalf of the Foundation for Science and Technology, through the Internationalisation Partnership Awards Scheme + (IPAS+) Grant Number IPAS-2023-051 and through FUSION: The

R&I Technology Development Programme 2018 project, Grant Number R&I-2017-033T (Project A-ROW).

## Conflict of interest

The authors have no conflicts of interest to declare that are relevant to the content of this article.

## ORCID iDs

Diego Di Brizzi  <https://orcid.org/0009-0006-9676-7821>  
 Serena Graziosi  <https://orcid.org/0000-0002-6103-9107>  
 Joseph N Grima  <https://orcid.org/0000-0001-5108-6551>  
 Alessandro Airoidi  <https://orcid.org/0000-0002-4938-3407>

## References

- [1] Jiao P, Mueller J, Raney J R, Zheng X and Alavi A H 2023 Mechanical metamaterials and beyond *Nat. Commun.* **14** 6004
- [2] Evans K E, Nkansah M A, Hutchinson I J and Rogers S C 1991 Molecular network design *Nature* **353** 124
- [3] Yang W, Li Z-M, Shi W, Xie B-H and Yang M-B 2004 Review on auxetic materials *J. Mater. Sci.* **39** 3269–79
- [4] Wojciechowski K W 1989 Two-dimensional isotropic system with a negative Poisson ratio *Phys. Lett. A* **137** 60–64
- [5] Lakes R 1987 Foam structures with a negative Poisson's ratio *Science* **235** 1038–40
- [6] Carneiro V H, Meireles J and Puga H 2013 Auxetic materials—a review *Mater. Sci.* **31** 561–71
- [7] Choi J B and Lakes R S 1992 Non-linear properties of polymer cellular materials with a negative Poisson's ratio *J. Mater. Sci.* **27** 4678–84
- [8] Coenen V L and Alderson K L 2011 Mechanisms of failure in the static indentation resistance of auxetic carbon fibre laminates *Phys. Status Solidi b* **248** 66–72
- [9] Sanami M, Ravirala N, Alderson K and Alderson A 2014 Auxetic materials for sports applications *Proc. Eng.* **72** 453–8
- [10] Lakes R S and Elms K 1993 Indentability of conventional and negative Poisson's ratio foams *J. Compos. Mater.* **27** 1193–202
- [11] Dudek K K, Wolak W and Grima J N 2019 Open impact resistance of composite magnetic metamaterials
- [12] Bezazi A and Scarpa F 2009 Tensile fatigue of conventional and negative Poisson's ratio open cell PU foams *Int. J. Fatigue* **31** 488–94
- [13] Choi J B and Lakes R S 1996 Fracture toughness of re-entrant foam materials with a negative Poisson's ratio: experiment and analysis *Int. J. Fract.* **80** 73–83
- [14] Imbalzano G, Tran P, Ngo T D and Lee P V S 2016 A numerical study of auxetic composite panels under blast loadings *Compos. Struct.* **135** 339–52
- [15] Hou S, Liu T, Zhang Z, Han X and Li Q 2015 How does negative Poisson's ratio of foam filler affect crashworthiness? *Mater. Des.* **82** 247–59
- [16] Alderson K L, Simkins V R, Coenen V L, Davies P J, Alderson A and Evans K E 2005 How to make auxetic fibre reinforced composites *Phys. Status Solidi b* **242** 509–18
- [17] Mohsenizadeh S, Alipour R, Shokri Rad M, Farokhi Nejad A and Ahmad Z 2015 Crashworthiness assessment of auxetic foam-filled tube under quasi-static axial loading *Mater. Des.* **88** 258–68



- [18] Allen T, Hewage T, Newton-Mann C, Wang W, Duncan O and Alderson A 2017 Fabrication of auxetic foam sheets for sports applications *Phys. Status Solidi b* **254** 1700596
- [19] Lorato A, Innocenti P, Scarpa F, Alderson A, Alderson K L, Zied K M, Ravirala N, Miller W, Smith C W and Evans K E 2010 The transverse elastic properties of chiral honeycombs *Compos. Sci. Technol.* **70** 1057–63
- [20] Alderson A, Alderson K L, Chirima G, Ravirala N and Zied K M 2010 The in-plane linear elastic constants and out-of-plane bending of 3-coordinated ligament and cylinder-ligament honeycombs *Compos. Sci. Technol.* **70** 1034–41
- [21] Chen C, Airolidi A, Caporale A M, Sala G and Yin X 2024 Impact response of composite energy absorbers based on foam-filled metallic and polymeric auxetic frames *Compos. Struct.* **331** 117916
- [22] Scarpa F 2008 Auxetic materials for bioprotheses [In the Spotlight] *IEEE Signal Process. Mag.* **25** 128–126
- [23] Luo Y M, He C, Tao Z, Hao J, Xu H H, Zhang Y, Zhang F and Ren X 2024 A surface-wave seismic metamaterial filled with auxetic foam *Int. J. Mech. Sci.* **262** 108715
- [24] Zeng J, Hu H and Zhou L 2017 A study on negative Poisson's ratio effect of 3D auxetic orthogonal textile composites under compression *Smart Mater. Struct.* **26** 065014
- [25] Meeusen L, Candidori S, Micoli L L, Guidi G, Stanković T and Graziosi S 2022 Auxetic structures used in kinesiology tapes can improve form-fitting and personalization *Sci. Rep.* **12** 13509
- [26] Dudek K K, Gatt R, Dudek M R and Grima J N 2018 Negative and positive stiffness in auxetic magneto-mechanical metamaterials *Proc. R. Soc. A* **474** 20180003
- [27] Dudek K K, Gatt R and Grima J N 2020 3D composite metamaterial with magnetic inclusions exhibiting negative stiffness and auxetic behavior *Mater. Des.* **187** 108403
- [28] Ma Y, Scarpa F, Zhang D, Zhu B, Chen L and Hong J 2013 A nonlinear auxetic structural vibration damper with metal rubber particles *Smart Mater. Struct.* **22** 084012
- [29] Wang Z, Zulifqar A and Hu H 2016 *Auxetic Composites in Aerospace Engineering Advanced Composite Materials for Aerospace Engineering* (Elsevier) pp 213–40
- [30] Choi J B and Lakes R S 1991 Design of a fastener based on negative Poisson's ratio foam *Cell. Polym.* **10** 205–12
- [31] Galea R, Farrugia P-S, Dudek K K, Attard D, Grima J N and Gatt R 2023 A novel design method to produce 3D auxetic metamaterials with continuous pores exemplified through 3D rotating auxetic systems *Mater. Des.* **226** 111596
- [32] Wojciechowski K W, Alderson A, Grima J N and Scarpa F 2020 Auxetics and other systems with “negative” characteristics *Phys. Status Solidi b* **257** 2000496
- [33] Brańka A C, Heyes D M and Wojciechowski K W 2009 Auxeticity of cubic materials *Phys. Status Solidi b* **246** 2063–71
- [34] Brańka A C, Heyes D M and Wojciechowski K W 2011 Auxeticity of cubic materials under pressure *Phys. Status Solidi b* **248** 96–104
- [35] Wang X-T, Wang B, Li X-W and Ma L 2017 Mechanical properties of 3D re-entrant auxetic cellular structures *Int. J. Mech. Sci.* **131–132** 396–407
- [36] Cheng X, Zhang Y, Ren X, Han D, Jiang W, Zhang X G, Luo H C and Xie Y M 2022 Design and mechanical characteristics of auxetic metamaterial with tunable stiffness *Int. J. Mech. Sci.* **223** 107286
- [37] Grima J N, Farrugia P S, Caruana C, Gatt R and Attard D 2008 Auxetic behaviour from stretching connected squares *J. Mater. Sci.* **43** 5962–71
- [38] Cabras L and Brun M 2016 A class of auxetic three-dimensional lattices *J. Mech. Phys. Solids* **91** 56–72
- [39] Grima J N, Attard D, Gatt R and Cassar R N 2009 A novel process for the manufacture of auxetic foams and for their re-conversion to conventional form *Adv. Eng. Mater.* **11** 533–5
- [40] Ngo T D, Kashani A, Imbalzano G, Nguyen K T Q and Hui D 2018 Additive manufacturing (3D printing): a review of materials, methods, applications and challenges *Composites B* **143** 172–96
- [41] Wang F 2018 Systematic design of 3D auxetic lattice materials with programmable Poisson's ratio for finite strains *J. Mech. Phys. Solids* **114** 303–18
- [42] Yang L, Harrysson O, West H and Cormier D 2015 Mechanical properties of 3D re-entrant honeycomb auxetic structures realized via additive manufacturing *Int. J. Solids Struct.* **69–70** 475–90
- [43] Zhang Z, Wen Q, Li P and Hu H 2022 Application of double arrowhead auxetic honeycomb structure in displacement measurement *Sens. Actuators A* **333** 113218
- [44] Mousanezhad D, Haghpanah B, Ghosh R, Hamouda A M, Nayeib-Hashemi H and Vaziri A 2016 Elastic properties of chiral, anti-chiral, and hierarchical honeycombs: a simple energy-based approach *Theor. Appl. Mech. Lett.* **6** 81–96
- [45] Grima J N, Alderson A and Evans K E 2005 Auxetic behaviour from rotating rigid units *Phys. Status Solidi b* **242** 561–75
- [46] Tabacu S, Predoiu P and Negrea R 2021 A theoretical model for the estimate of plateau force for the crushing process of 3D auxetic anti-tetra chiral structures *Int. J. Mech. Sci.* **199** 106405
- [47] Babaee S, Shim J, Weaver J C, Chen E R, Patel N and Bertoldi K 2013 3D soft metamaterials with negative Poisson's ratio *Adv. Mater.* **25** 5044–9
- [48] Yao Y, Wang L, Li J, Tian S, Zhang M and Fan Y 2020 A novel auxetic structure based bone screw design: tensile mechanical characterization and pullout fixation strength evaluation *Mater. Design* **188** 108424
- [49] Ren X, Shen J, Tran P, Ngo T D and Xie Y M 2018 Auxetic nail: design and experimental study *Compos. Struct.* **184** 288–98
- [50] Kuskun T, Jerzy S and Ali K 2021 Experimental and numerical analysis of mounting force of auxetic dowels for furniture joints *Eng. Struct.* **226** 111351
- [51] Kudela J and Matousek R 2022 Recent advances and applications of surrogate models for finite element method computations: a review *Soft Comput.* **26** 13709–33
- [52] Sadeghifar M, Javidikia M, Songmene V and Jahazi M 2020 Finite element simulation-based predictive regression modeling and optimum solution for grain size in machining of Ti6Al4V alloy: influence of tool geometry and cutting conditions *Simul. Model. Pract. Theory* **104** 102141
- [53] Athreya S, Weinschenk A, Steinlehner F, Budnick D, Worswick M, Volk W and Huhn S 2021 Parametric shape optimization of stretch webs in a progressive die process using a neural network surrogate model *IOP Conf. Ser.: Mater. Sci. Eng.* **1157** 012081
- [54] Rikards R, Abramovich H, Kalnins K and Auzins J 2006 Surrogate modeling in design optimization of stiffened composite shells *Compos. Struct.* **73** 244–51
- [55] Smith M 2009 *ABAQUS/Standard User's Manual, Version 6.9* (Dassault Systèmes Simulia Corp)
- [56] Janbaz S, Noordzij N, Widayati D S, Hagen C W, Fratila-Apachitei L E and Zadpoor A A 2017 Origami lattices with free-form surface ornaments *Sci. Adv.* **3** ea01595
- [57] Jiang W, Ren X, Wang S L, Zhang X G, Zhang X Y, Luo C, Xie Y M, Scarpa F, Alderson A and Evans K E 2022 Manufacturing, characteristics and applications of auxetic foams: a state-of-the-art review *Composites B* **235** 109733